Received: 18 November 2023 | Revised: 15 March 2024 | Accepted: 8 April 2024

DOI: 10.1002/pen.26764

RESEARCH ARTICLE

POLYMER ENGINEERING AND SCIENCE WILEY

Utilization of cross-correlation function for assessment of replication quality in ultrasonic embossing of microchannels on polymethyl methacrylate

Ender Yildirim[1,2] | **Mert Kerem Ulku**[1] | **M. A. Sahir Arikan**[1]

[1]Mechanical Engineering Department, Middle East Technical University, Ankara, Turkey

[2]METU MEMS Center, Ankara, Turkey

Correspondence
Ender Yildirim, Mechanical Engineering Department, Middle East Technical University, Ankara, Turkey.
Email: yender@metu.edu.tr

Present addresses
Mert Kerem Ulku, Department of Biomedical Engineering, Texas A&M University, College Station, Texas 77843, USA; and Center for Remote Health Technologies and Systems, Texas A&M Engineering Experiment Station, College Station, Texas 77843, USA.

Funding information
Türkiye Bilimsel ve Teknolojik Araştırma Kurumu, Grant/Award Number: 121M427; Orta Doğu Teknik Üniversitesi, Grant/Award Number: GAP-302-2018-2757

Abstract

Ultrasonic embossing—a process where a horn vibrating at 20–30 kHz compresses on a thermoplastic substrate sitting on a mold to replicate the features on the mold to the substrate—is a promising method for fabricating microchannels on thermoplastics due to reduced cycle time and relatively low equipment cost. Replication quality in ultrasonic embossing has been investigated in the literature by primarily referring to the replication depth. However, this approach does not fully reflect the fidelity between the mold and the replicated feature, especially at the side walls, which are typically designed to be vertical in microchannels. We propose using cross-correlation—a method that quantifies the similarity between two signals by measuring the overlap of their patterns—between the derivative of the mold profile and the embossed profile as a figure of merit that accurately reflects the fidelity of the side wall. For testing purposes, we embossed straight microchannels on polymethyl methacrylate (PMMA) using micron-scaled protrusions on a brass mold fabricated by CNC milling. The mold comprised 100, 300, and 1000-μm-wide protrusions of same designed height of 300 μm, resulting in aspect ratios (AR) of 3, 1, and 1/3, respectively. Cross-correlations between the derivatives of the profiles ranged between 0.50 and 1.00, while cross-correlations between the profiles were greater than 0.97 in all cases, showing the sensitivity imposed by utilizing the derivatives. Setting average of all cross-correlation values (0.8) as the quality threshold, we observed that high AR (3) features were replicated at low quality, while low AR (1/3) features were replicated at high quality, regardless of the process parameters. In replicating unit AR features, the process parameters were observed to affect the quality, where the combination of vibration time and pressure was the most significant compared to individual effects of the parameters.

Highlights

- Parameters' effect on replication of varied aspect ratio features was assessed.
- Assessment was carried out by cross-correlating mold and channel profiles.

- Cross-correlating derivatives of profiles provide a more sensitive means.
- General rules for replication quality in ultrasonic embossing were driven.

KEYWORDS

cross-correlation, microchannel, polymethyl methacrylate, ultrasonic embossing

1 | INTRODUCTION

Patterning micro- and mini-features on thermoplastic substrates is a primary concern, especially in developing microfluidic devices mainly used in life sciences for analytical, diagnostic, or therapeutic purposes. The microfluidic devices are composed of microchannels and reservoirs with at least one characteristic dimension (typically the height or the width of features), typically less than 1 mm. Silicone molding[1] and micromilling[2] are the common methods used for prototyping purposes. In addition to these methods, recently, there has been considerable progress toward prototyping by additive manufacturing (i.e., 3D printing).[3] On the other hand, for high-volume manufacturing for commercial purposes, injection molding[4,5] is the standard method. For medium volume, hot embossing process appears as a well-established alternative.[6] Variations of hot embossing methods, such as infrared-assisted hot embossing,[7] induction-assisted hot embossing,[8] and ultrasonic embossing,[9,10] have also been developed mainly to decrease the cycle time. Among these variants, ultrasonic embossing process[11] appears as a promising alternative, especially for medium- to high-volume production of plastic microfluidics, since it reduces the cycle time for patterning the microfeatures on a single microfluidic device to the order of 10^1 s,[12] which is comparable to typical cycle times in injection molding. In addition, the process can be carried out on an ultrasonic welding machine, which is typically less costly than an injection molding machine.[13]

In ultrasonic embossing, a horn vibrating at 20–30 kHz frequencies compresses the thermoplastic substrate against a mold. Figure 1 illustrates the process. In the first stage of the process, the horn presses the substrate against the mold without vibration. The horn starts vibrating in the next stage while pressing on the substrate. Ultrasonic vibrations induce friction at the horn–substrate and substrate–mold interfaces. As the features on the mold introduce surface irregularities, the friction is more pronounced at the substrate–mold interface, resulting in rapid heating where the features are posed. The heat increases the temperature in the process-affected zone above the glass transition temperature of the substrate material[13] within a short timeframe, and the softened substrate is deformed. In the following stage, the vibration ceases, and the substrate cools down. Following this hold period, the horn is removed, and the substrate is released.

Comprehensive studies have been carried out to explain the underlying physics of the process,[13–15] and the process has been successfully applied to the manufacturing of microfluidic channels,[13–16] optical diffusers,[17] and even circuit boards.[18,19] Several other studies have investigated the effect of the process parameters on replication quality. Qi et al.[20] investigated the effect of process parameters on the uniformity and depth of the replicated microstructures, finding that increased vibration time significantly affected the replication depth. They also observed that higher pressure improved depth, but excessive pressure led to a reduction in replication depth. Mekaru et al.[9] confirmed Qi et al.'s findings through qualitative examination using an optical microscope, arriving at the same conclusions regarding the effect of pressure and vibration time.[9] Zhu et al.[21] reached a similar conclusion, adding that excessive

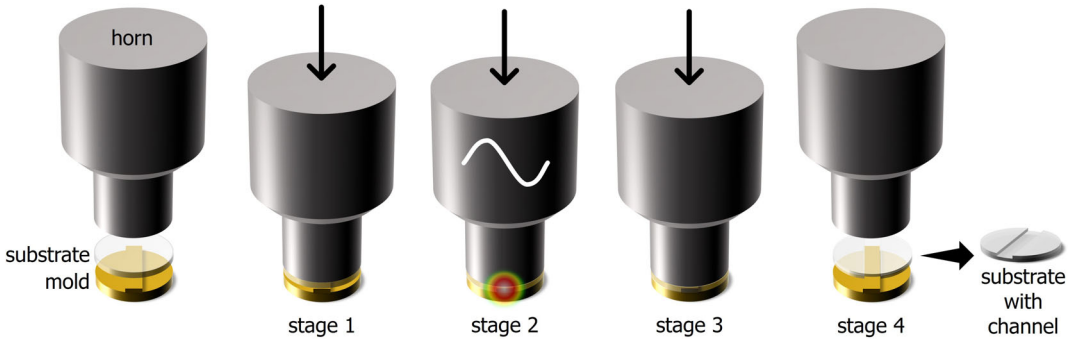

FIGURE 1 Illustration of the ultrasonic embossing process.

vibration time negatively affects the replication quality, by comparing the depth of replicated features with the mold. In another study, Liu et al.[17] utilized the deviation between replicated feature height at different locations on the substrate as the figure of merit to characterize the process, and in contrast to the findings in Reference [9], the authors concluded that higher pressure would result in better replicability. Similarly, they argued that increasing the vibration time would result in better replication. However, they also stated that overtime might cause overmelting of the substrate, and replicability might decrease. Same findings were also deduced by Liu et al.,[12] where the authors examined the quality by referring to the depths of the replicated features. Fang-Yu et al.[22] have reached the same conclusion, by utilizing the height ratio, defined as the ratio of the replicated pattern height to that of the mold, as the figure of merit. In addition, they have concluded that the vibration time is the most influential factor on the replication quality. Variants of ultrasonic embossing, where the mold and the substrate were preheated[23] or a hot plate was utilized as an additional heat source to assist the process,[24] were also investigated. In Reference [23], the authors utilized the average and standard deviation of the depths of a series of replicated features as indicators and concluded that vibration amplitude, the vibration time, and hot plate temperatures as the most effective factors on replication uniformity while increasing the hold time and pressure were observed to improve the replication quality. In Reference [24], feature depths were utilized as a figure to deduce that the vibration amplitude and the thermal-assisted temperature are the most effective on replication quality.

Ultrasonic embossing emerged as a result of efforts to decrease the cycle time compared to the conventional hot embossing process. On the other hand, as investigated in the abovementioned studies, the research is mainly directed toward optimizing the process. The abovementioned studies commonly concluded that vibration time is the most effective parameter in ultrasonic embossing. It was also stated commonly that the delay time is not an essential factor in the process. As opposed to delay time, increasing the hold time was observed to improve the replication quality. On the other hand, there was no common ground for the effect of the pressure applied on the substrate by the horn. Some of the studies claim that increasing pressure improves replicability,[12,17,22] while it is stated that excessive pressure reduces the replication quality.[9,21] The difference between the conclusions in different studies might be caused by the difference in the feature dimensions tested or the range of process parameters investigated. On the other hand, it should also be noted that the metrology aspect was often overlooked as mostly a single dimension—depth—of the replicated features was used as the figure of merit. Table 1 summarizes the literature investigating the replication quality in ultrasonic embossing by referring to the figures of merit to quantify the replication quality. Here, it should be noted that the aim is to replicate not only the depth but the entire profile of the features. In addition, specifically in replicating microfeatures, sidewall geometry is a valuable indicator in optimizing the processes,[25] which was not considered in any of the studies. Therefore, we claim that replicated feature's profile and its fidelity to the targeted profile should be examined entirely, with a focus on the sidewalls, for a precise assessment.

Considering the metrology aspect, various approaches have been employed in other mold-based plastic micromanufacturing processes. Gülçür et al.[26] devised a custom imaging setup to capture high-resolution images of injection molded microneedles, using these images to quantify height as the performance metric. Similarly, in assessing replication quality in micro-injection molding, Vera et al.[27] utilized sub-micrometer-sized ripples on the mold, employing atomic force microscopy to measure three-dimensional surface profiles of these ripples on both the mold and the replicate. Then, they conducted Fourier analysis to calculate the spatial frequencies and compared the power spectral density peaks of the mold and the replicate to establish a replication rate as a figure of merit. Piccolo et al.[28] utilized the ratio between the surface roughness of the mold and the molded part, measured by atomic force microscopy, as an indicator of quality to assess the replication in micro-injection molding. However, none of these methods offer a means to assess the replication of microfeatures, particularly microchannels, where characterization of the side wall is especially vital.

In this paper, we assess the quality of replication of microchannels with intended vertical side walls fabricated by ultrasonic embossing by using the cross-correlation function. Cross-correlation is a commonly used tool to determine the similarity between two time series in signal processing. In manufacturing, the utilization of cross-correlation has been presented for tool wear monitoring purposes.[29–31] The method was also utilized for the assessment of the replication of 3D-printed rough surface topographies in different polymers by injection molding and polymer casting.[32] Kumar et al.[33] employed the same approach for characterizing replica molding of natural surfaces. Although cross-correlation between the mold and the replication profiles was justified for assessment of replication of generated rough surfaces, an improved method that is more sensitive to local slopes is required in assessing the replication quality of microchannels as the side walls of the microchannels are often designed to be vertical with ideally infinite slope. As an improved method, we propose to utilize the derivatives of the fabricated and

TABLE 1 Figures utilized in the literature to assess replication quality in ultrasonic embossing.

Reference	Geometry	Scale	Aspect ratio (AR)[a]	Measure of replication quality
Qi et al.[20]	Convex- and concave-tapered grooves	Width and depth/height 10^1 μm	~1/3–1	Replication depth
Mekaru et al.[9]	Concave quadrangular pyramids	Width 10^2–10^3 μm Height 10^1–10^2 μm	~1/5–1	Ratio of the number of successfully replicated patterns to the number of all patterns evaluated by visual inspection
Zhu et al.[21]	Square cavities in the form of a checkerboard	Width and depth 10^2 μm	~1/2	Replication depth
Liu et al.[17]	Array of triangular grooves	Width and depth 10^2 μm	~1/4	Deviation of the embossed feature height across the substrate
Liu et al.[12]	Array of pyramids	Width and height 10^3 μm	1	Standard deviation of the depth of embossed features from the nominal depth
Fang-Yu et al.[22]	Array of rectangular grooves	Width 10^0 μm Depth 10^{-1} μm	1/10	Ratio of the height of the embossed features to that of the mold.
This study	Straight protrusions of rectangular cross-section	Width 10^2–10^3 μm Depth 10^2 μm	~1/3–3	Cross-correlation between the profiles and derivative of the profiles of the mold and the replicate

[a]Aspect ratio (AR) is defined as the ratio of the feature depth or height to the feature width.

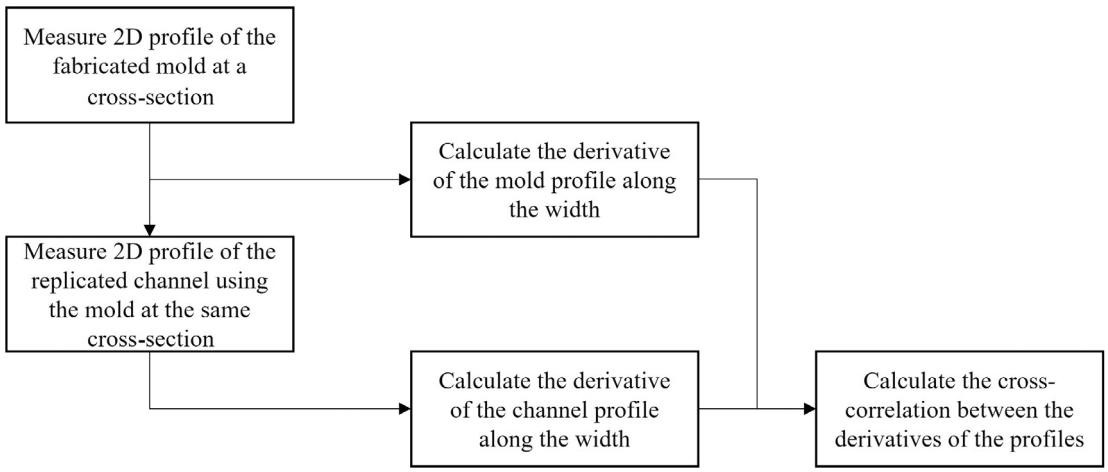

FIGURE 2 Flowchart showing the improved cross-correlation calculation for assessing the replication quality.

target profiles in computing the cross-correlation. Figure 2 shows the flowchart for assessing the replication quality by utilizing the improved cross-correlation calculation. For testing purposes, we fabricated a brass mold including three protrusions in the form of straight lines of varying widths by machining. The protrusions were replicated on polymethyl methacrylate (PMMA) by ultrasonic embossing to form straight channels. The vibration time and the pressure were altered to observe their effects on replication quality. Replication quality was assessed by utilizing both the cross-correlation between the profiles and the cross-correlation between the derivatives of the profiles to prove the sensitivity of the proposed method. The effect of the process parameters on replication quality was investigated by using the proposed method.

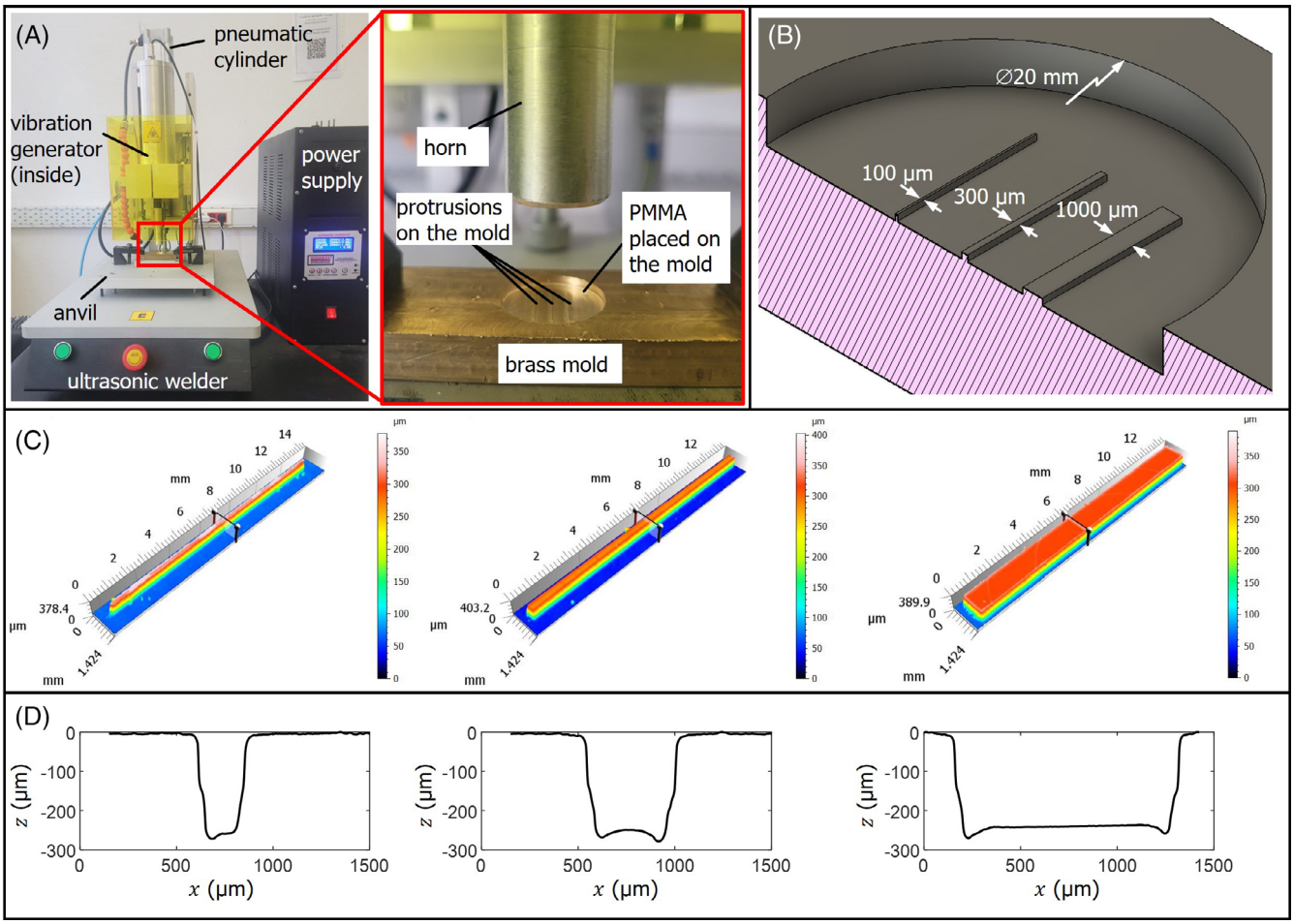

FIGURE 3 (A) Ultrasonic embossing setup showing the components on the ultrasonic welder and details of the horn and the mold. (B) The features on the mold in the shape of straight-line protrusions. (C) Three-dimensional profiles of the protrusions and (D) the negative of the profiles measured at the midpoint of the protrusions representing the target profiles.

2 | EXPERIMENTAL

2.1 | Ultrasonic embossing setup

In the experiments, we utilized a 600-W benchtop ultrasonic welder (SNKW-P1-3006, Sonikel Ultrasonics, Istanbul, Türkiye) to provide ultrasonic vibrations at 30 kHz. A brass mold vertically aligned with the horn was mounted on the anvil. Figure 3A shows the setup.

The mold was composed of protrusions in the form of straight lines of width 100, 300, and 1000 µm. All protrusions were designed to have the same height of 300 µm, resulting in aspect ratios (AR) of 3, 1, and 1/3 for 100-µm-wide, 300-µm-wide, and 1000µm-wide protrusions. We placed the protrusions on the mold sufficiently distant from each other and the edges of the mold, considering the width of the process-affected zone in ultrasonic embossing,[13] to ensure that the material flow at the vicinity of each protrusion was not affected from each other. The protrusions were machined on a brass plate in a 20-mm-diameter cylindrical recess, where disk-shaped PMMA substrates could be placed. A benchtop CNC milling machine (PROXXON MF70 CNC Ready, PROXXON GmbH, Föhren, Germany) was used for machining the mold. A 2-mm-diameter coated carbide end mill rotating at 4000 rpm, which is the maximum spindle speed provided by the machine tool, was fed at 100 mm/min with a maximum depth of cut of 0.3 mm to prevent failure of the tool during machining. To eliminate the burrs, the part program was executed again without dismounting the machined brass plate from the worktable. This process involved maintaining a zero depth of cut exclusively to remove any residual burrs on the corners. Three-dimensional profiles of the protrusions (Figure 3C) were measured using a laser scanning confocal digital microscope (VK40, Keyence Co., Osaka, Japan). Profile measurements showed that the height of the protrusions (Figure 3C) was about 250 µm on average. Negatives of two-dimensional profiles of the

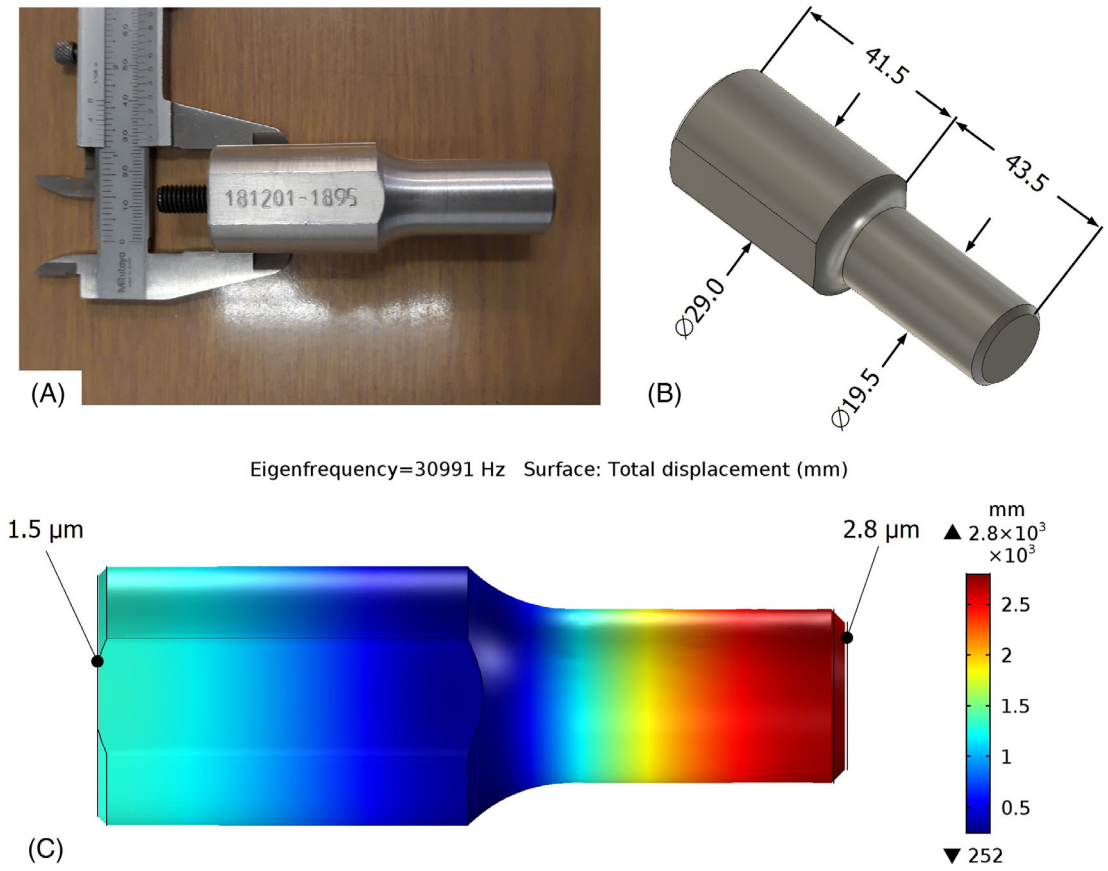

FIGURE 4 (A) The horn installed on the ultrasonic welder and (B) its dimensions. (C) The modal analysis result showing the vibration mode at 30991 Hz and the vibration amplitude at the horn's tip and root.

protrusions measured at their midpoints, as illustrated in Figure 3C, were defined as the target channel profiles (Figure 3D).

To prepare the substrate, we cut a 1-mm-thick polymethylmethacrylate (PMMA) sheet into 20-mm-diameter disks, considering the tip diameter of the horn and the pocket on the mold, by using a router (LPKF ProtoMat S105, LPKF Laser & Electronics, Garbsen, Germany).

A stepped cylindrical horn machined from AA7075 aluminum stock was used in the experiments. The horn and its dimensions are shown in Figure 4. To determine the amplification factor (ζ), which is the ratio of the vibration amplitude at the tip of the horn (η_h) to that at its root (η_t) ($\zeta = |\eta_h/\eta_t|$), we carried out a modal analysis using COMSOL Multiphysics. The result of the modal analysis is shown in Figure 4C, indicating that 1.5 µm amplitude at the root of the horn is amplified to 2.8 µm, resulting in an amplification factor of 1.87. Numerical results were verified by measuring the amplitude of the vibration generated by the piezoelectric transducer and vibration amplitude at the tip of the horn mounted at the transducer using a laser Doppler vibrometer (Polytec CLV 2534, Polytec Inc., Irvine, CA, USA).

2.2 | Design of experiments

A full-factorial experiment was designed to investigate the effect of the pressure (p) and the vibration time (t_v) on replication quality. The pressure was generated by pressurizing a 40-mm inner diameter pneumatic cylinder on the ultrasonic welder. Considering the capabilities of the ultrasonic welder as stated by its manufacturer, we decided on 4, 5, and 6 bars as three levels of pneumatic pressure, which correspond to 500, 625, and 750 N compressive force, respectively. Noting the tip diameter of the horn, we calculated the pressure exerted on the substrate by the horn as 1.6, 2.4, and 3.2 MPa. Based on the preliminary tests and the findings of our previous work on ultrasonic embossing,[13] the ultrasonic vibration time was set to 3, 5, and 7 s. The hold time was kept constant at 5 s. Table 2 presents the full-factorial experiment matrix. The experiments in Table 2 were carried out in random order, and each experiment was replicated three times.

To extract the two-dimensional profiles of the replicated channels, we cut the samples into two by using a blade along the diameter passing through the

TABLE 2 Experiments to determine the effect of pressure and vibration time on replication quality.

Experiment	Pressure, p (MPa)	Vibration time, t_v (s)
1	1.6	3
2	2.4	3
3	3.2	3
4	1.6	5
5	2.4	5
6	3.2	5
7	1.6	7
8	2.4	7
9	3.2	7

Note: The experiments were replicated three times. The hold time was 5 s in all experiments.

midpoint of the channels, as illustrated in Figure 5A. The cut planes on one-half of each sample were then polished by wet sanding using 1000-grit sandpaper. After polishing, the cut planes were viewed under a stereomicroscope to capture the cross-section of each channel. Before further processing, the microscope was calibrated using a known scale at the same focal distance. The captured cross-section images were then cropped to a region of interest (ROI) such that only the channels and the plateaus on the pileup regions on both sides of the channels are included (Figure 5B). The cropped images were then converted into binary images (Figure 5C). Finally, the boundaries between the black and white regions were detected to obtain the two-dimensional profiles of the channels (Figure 5D). The pixel coordinates of the boundaries were extracted and scaled to convert the x and y coordinates of the profiles to μm for further analysis (Figure 5E). Open-source image processing tool ImageJ was used for the analysis of the images.

2.3 | Cross-correlation between the profiles

To quantify the replication quality, we first calculated the cross-correlation (r) (Equation 1) between the target channel profiles, $y_m(x)$ (which are the negatives of two-dimensional profiles of the protrusions on the mold shown in Figure 3D), and the profiles of the fabricated channels, $y_c(x)$ (as illustrated in Figure 5E). In Equation (1), $\bar{y}_m$ and $\bar{y}_c$ represent the mean of the target and fabricated channel profiles, respectively,

$$r(\delta) = \frac{\sum (y_m(x) - \bar{y}_m)(y_c(x-\delta) - \bar{y}_c)}{\sqrt{\sum (y_m(x) - \bar{y}_m)^2}\sqrt{\sum (y_c(x-\delta) - \bar{y}_c)^2}}. \quad (1)$$

In calculating the cross-correlation, the deviation of the target channel profile and the deviation of the fabricated channel profile from their respective means are elementwise multiplied and summed up along the horizontal axis x (note the terms that appear in the numerator in Equation (1)). Therefore, if the fabricated channel profile matches exactly with the targeted channel profile, then this summation yields a relatively large value, which equals the sum of the squares of the deviation of either profile from its mean. This sum is normalized by dividing it by the square root of the sum of squares (RSS) of deviation of both targeted and fabricated channel profiles from their respective means (note the terms in the denominator in Equation (1)). Thus, if the fabricated and the targeted profiles are the same, the denominator will be equal to the numerator in Equation (1) and the cross-correlation value will be unity, which is the maximum value it can take.

On the other hand, it should be noted that since the origins of the horizontal axes of the target channel profiles (Figure 3D) and fabricated channel profiles (Figure 5E) do not necessarily coincide, as they are measured separately. As a result, there would be net shifts between the fabricated channel profiles and the target profile along the x-axis by arbitrary amounts (δ), as illustrated in Figure 6. To determine this arbitrary amount of shift δ, we calculated the cross-correlation (r) given by Equation (1) for all possible values of shift δ. The value of δ resulting in the highest r was determined as the shift and the corresponding value of r as the cross-correlation between the fabricated and target channels.

2.4 | Cross-correlation between the derivatives of the profiles

Although most of the studies consider the replication depth or depth-related measures to characterize the replication quality (Table 1), it is common in the embossing of microfluidic devices that the side walls are not perfectly replicated either due to incomplete flow of material into the mold or recovery of the material after the process[34,35] A method, which is sensitive to the side wall fidelity, is to modify Equation (1) by taking the derivative of both target and fabricated channel profiles so that the discrepancy between the slopes of the profiles is amplified,

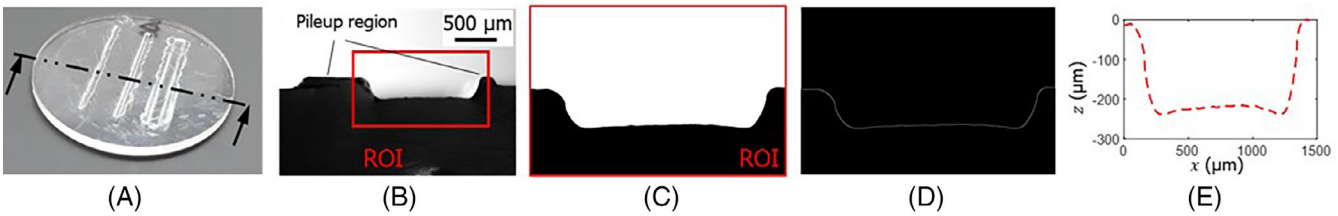

FIGURE 5 (A) The axis along which the samples were cut, arrows indicating the direction of viewing. (B) Sample image captured under the stereo microscope indicating the region of interest (ROI). (C) The binary representation of the ROI. (D) The boundary between black and white regions in ROI saved as (E) a two-dimensional profile of the fabricated channel.

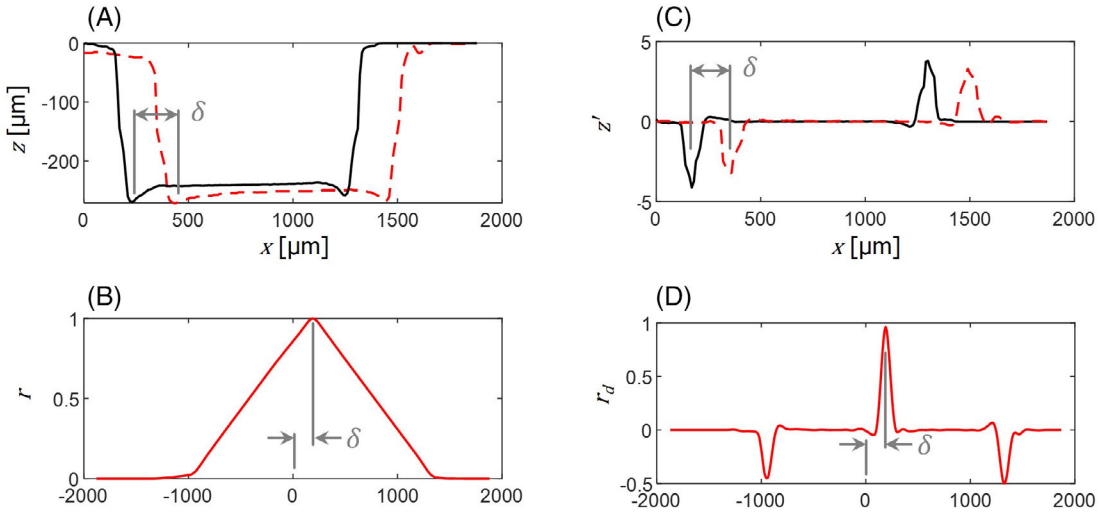

FIGURE 6 (A) Target (full black line) and fabricated (dashed red line) channel profiles, and (B) corresponding cross-correlation (r) for all possible amounts of shifts. (C) Derivatives of the target (full black line) and fabricated (dashed red line) channel profiles, and (D) corresponding cross-correlation (r_d) for all possible amounts of shifts.

$$r_d(\delta) = \frac{\sum \left(y'_m(x) - \overline{y}'_m\right)\left(y'_c(x-\delta) - \overline{y}'_c\right)}{\sqrt{\sum \left(y'_m(x) - \overline{y}'_m\right)^2}\sqrt{\sum \left(y'_c(x-\delta) - \overline{y}'_c\right)^2}}, \quad (2)$$

where $r_d(\delta)$ represents the cross-correlation between the derivatives of the profiles; $y'_m(x)$ represents the derivative of the target channel profile with respect to the horizontal axis x, and $\overline{y}'_m$ is its mean along x; and similarly, $y'_c(x)$ represents the derivative of the fabricated channel profile with respect to x and $\overline{y}'_c$ is its mean along x.

To calculate the cross-correlations $r(\delta)$ and $r_d(\delta)$, firstly the target and fabricated channel profiles were resampled so that both arrays have the same length. The sampling width along x-axis was selected such that 100 measurements were taken across the designed width of the channels. As a result, the sampling width was selected as 1, 3, and 10 μm for the designed channel width of 100, 300, and 1000 μm, respectively.

3 | RESULTS AND DISCUSSION

3.1 | Characterization of the horn

Modal analysis using COMSOL Multiphysics proved that the horn has an axial vibration mode at 30 kHz. The simulation showed that the displacement amplitude in the axial direction at the tip was 2.8 μm compared to that of 1.5 μm at the root, resulting in an amplification factor of $\zeta = 2.8/1.5 = 1.87$ (Figure 4C). The numerically calculated amplification factor was verified by laser Doppler vibrometry. The output voltage of the vibrometer at the transducer tip was measured as 1.5 V, while 2.5 V output voltage was measured at the horn tip, yielding an amplification factor of $\zeta = V_{\text{out},h}/V_{\text{out},t} = 2.5/1.5 = 1.67$.

The scheme for the experimental characterization of the horn by utilizing laser Doppler vibrometry measures the vibration amplitude generated by the transducer and that at the horn tip. However, we observed that the measurement was greatly affected by the condition of

TABLE 3 The averages of r and r_d computed for three replicates of each experiment.

		Pressure, p(MPa)		
		1.6	**2.4**	**3.2**
Channel width: 1000 μm, aspect ratio (AR): 1/3				
Vibration time, t_v (s)	3	$r = 0.996 \pm 0.000$	$r = 0.998 \pm 0.002$	$r = 0.997 \pm 0.003$
		$r_d = 0.899 \pm 0.024$	$r_d = 0.929 \pm 0.054$	$r_d = 0.935 \pm 0.029$
	5	$r = 0.996 \pm 0.000$	$r = 0.996 \pm 0.001$	$r = 0.995 \pm 0.001$
		$r_d = 0.927 \pm 0.008$	$r_d = 0.889 \pm 0.016$	$r_d = 0.874 \pm 0.025$
	7	$r = 0.998 \pm 0.001$	$r = 0.998 \pm 0.001$	$r = 0.998 \pm 0.000$
		$r_d = 0.942 \pm 0.063$	$r_d = 0.933 \pm 0.057$	$r_d = 0.955 \pm 0.016$
Channel width: 300 μm, aspect ratio (AR): 1				
Vibration time, t_v (s)	3	$r = 0.998 \pm 0.001$	$r = 0.995 \pm 0.001$	$r = 0.992 \pm 0.006$
		$r_d = 0.859 \pm 0.049$	$r_d = 0.841 \pm 0.031$	$r_d = 0.790 \pm 0.030$
	5	$r = 0.984 \pm 0.006$	$r = 0.994 \pm 0.001$	$r = 0.990 \pm 0.008$
		$r_d = 0.653 \pm 0.123$	$r_d = 0.808 \pm 0.033$	$r_d = 0.778 \pm 0.016$
	7	$r = 0.997 \pm 0.001$	$r = 0.995 \pm 0.003$	$r = 0.998 \pm 0.000$
		$r_d = 0.850 \pm 0.051$	$r_d = 0.820 \pm 0.054$	$r_d = 0.886 \pm 0.025$
Channel width: 100 μm, aspect ratio (AR): 3				
Vibration time, t_v (s)	3	$r = 0.993 \pm 0.002$	$r = 0.992 \pm 0.001$	$r = 0.990 \pm 0.003$
		$r_d = 0.646 \pm 0.010$	$r_d = 0.627 \pm 0.069$	$r_d = 0.625 \pm 0.147$
	5	$r = 0.990 \pm 0.011$	$r = 0.993 \pm 0.003$	$r = 0.973 \pm 0.006$
		$r_d = 0.572 \pm 0.062$	$r_d = 0.755 \pm 0.044$	$r_d = 0.619 \pm 0.049$
	7	$r = 0.983 \pm 0.012$	$r = 0.971 \pm 0.020$	$r = 0.983 \pm 0.014$
		$r_d = 0.561 \pm 0.084$	$r_d = 0.512 \pm 0.056$	$r_d = 0.607 \pm 0.086$

Note: The uncertainty presented is the standard deviation.

whether the transducer or the horn was mechanically loaded or not. It should be noted that measuring the vibration amplitudes at the root and the tip of the horn under operating conditions for characterization purposes remains a challenge.

3.2 | Ultrasonic embossing experiments

Table 3 presents the cross-correlation values r and r_d based on the target and fabricated channel profiles and their derivatives, respectively, for different process parameters (the pressure p and the vibration time t_v). Fabricated channel profiles compared to the target channel profiles for one set of experiments are also presented in Figure 7.

Table 3 shows that the average r (cross-correlation between the target and fabricated profiles) was mostly greater than 0.99 in replicating all channels. Examining Figure 7 reveals that in many cases, only the third significant figure in r is affected by how the fabricated channel profile complies with the targeted profile. For instance, r was calculated to be greater than 0.998 in replicating 300 μm-wide channels under 3.2 MPa pressure for 7 s (Figure 7B-ix), where even the beaks at the edges of the protrusion could be replicated. In replicating the same geometry by applying 7 s vibration time under 1.6 MPa pressure (Figure 7B-vii), there is a considerable "swallowtail" defect (defined as the unfilled corner at the root of the protrusion[35]). However, r was only 0.001 less (0.997) in comparison with the case shown in Figure 7B-ix. This indicates that although the cross-correlation between the target and fabricated profiles (r) can capture the defects in the replication, it cannot be considered a figure sensitive to the deviation between the target and fabricated profiles. On the other hand, the cross-correlation between the derivatives of the target and fabricated profiles (r_d) provides a quite sensitive figure for assessing the replication quality. It should be noted that r_d were computed as 0.889 and 0.830 for the same cases shown in Figure 7B-ix and vi, respectively. In conclusion, the swallowtail defect caused approximately 7% change in r_d (0.889 compared to 0.830), while the change was only about 0.1% in r (0.998 compared to 0.997) for the same case, which shows the sensitivity improved by utilizing the derivatives of the profiles in the calculation of the cross-correlation.

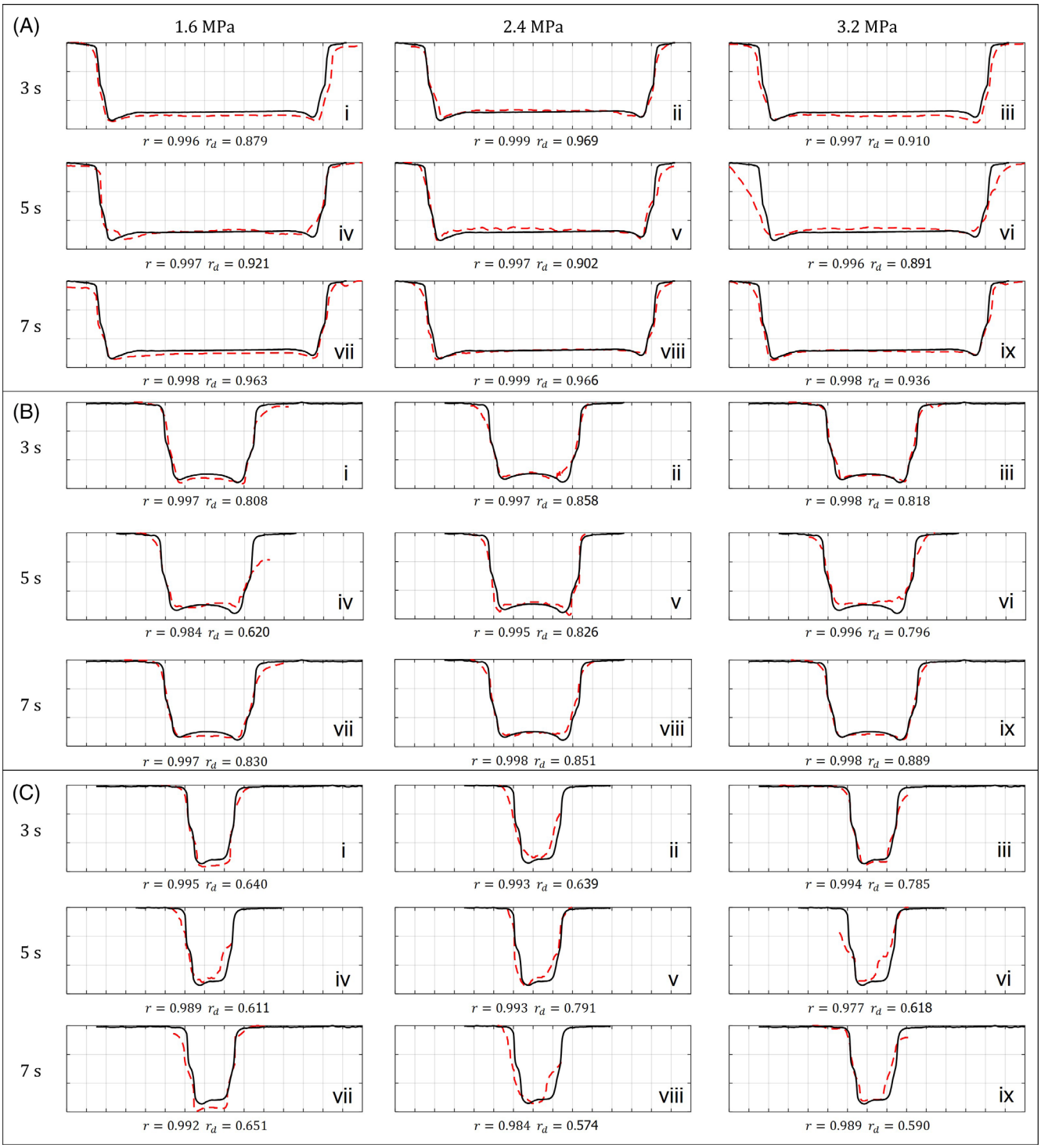

FIGURE 7 Comparison of the target (full black lines) and the fabricated profiles (dashed red lines) for (A) 1000-μm-wide channels (AR: 1/3), (B) 300-μm-wide channels (AR: 1), (C) 100-μm-wide channels (AR: 3), measured in one set of experiments. Both horizontal and vertical grid spacings are 100 μm.

To investigate the impact of utilizing the derivatives more in detail, we carried out a statistical analysis revealing the effect of parameters on both r and r_d.

Figure 8 illustrates the main effect plots and interaction plots considering cross-correlations based on the profiles (r). Initial inspection of Figure 8 depicts that the replication quality, as indicated by the cross-correlation (r), changes slightly with the channel width and aspect ratio. Figure 8 illustrates that average replication quality peaks with $r = 0.997$ for 1000-μm-wide channels

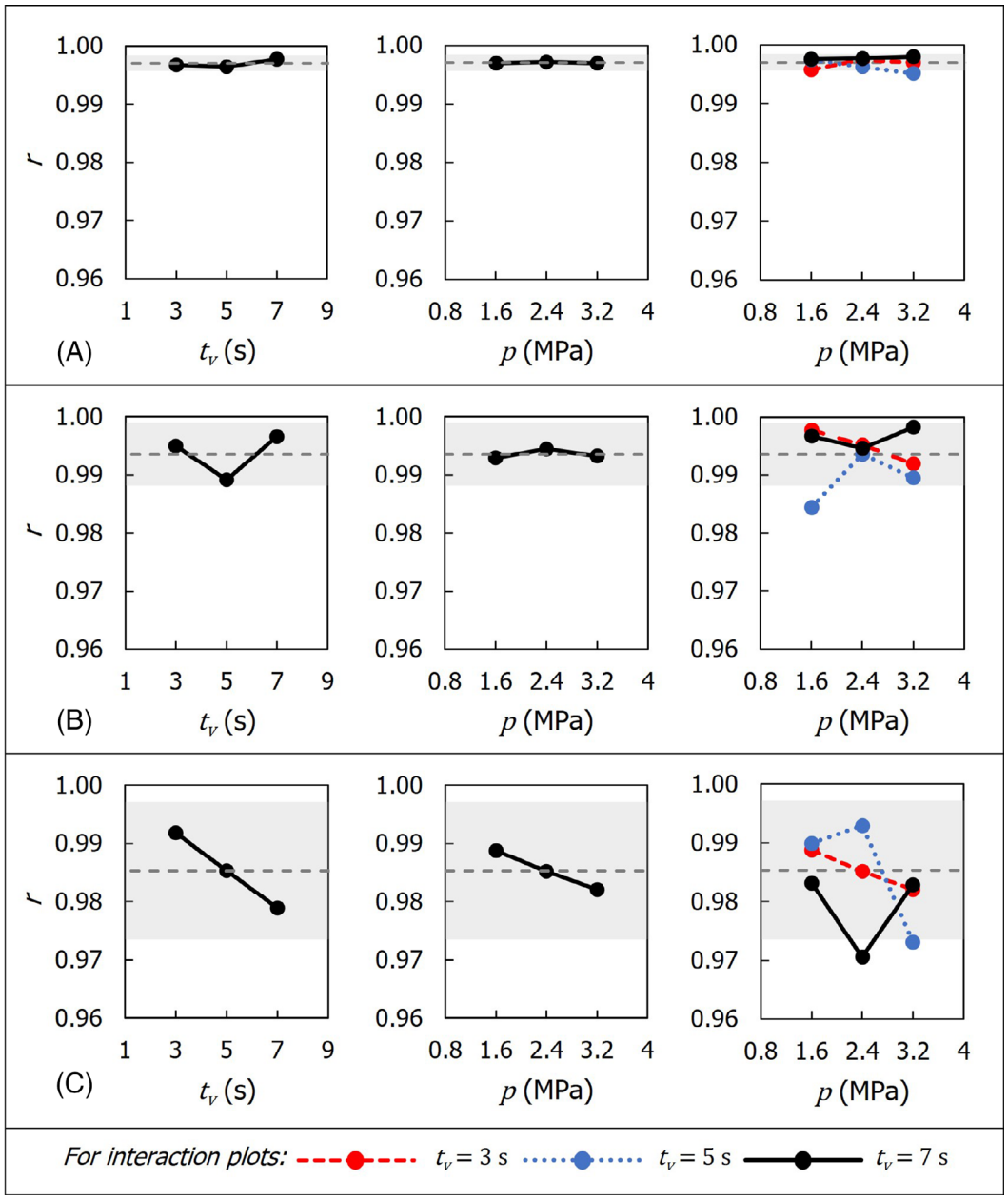

FIGURE 8 Main effects and interaction plots showing the relation between the cross-correlation *r* and the process parameters for (A–C) 1000-μm-wide channels (AR: 1/3), (D–F) 300-μm-wide channels (AR: 1), and (G–I) 100-μm-wide channels (AR: 3). Dashed lines indicate the average of the cross-correlation values for each channel width, while the gray band around the average indicates the standard deviations.

(AR = 1/3), while it is the least with $r = 0.985$ for 100-μm-wide channels (AR = 3). There is also a notable variation between how the parameters affect the replication quality across different channel widths and aspect ratios. Examining Figure 8A reveals that increasing the vibration time leads to a marginal reduction in the replication quality for embossing 1000-μm-wide channels (AR = 1/3). However, further extending the vibration time enhances the replication quality. In contrast, an initial increase in pressure results in a slight increase in the replication quality, but a subsequent rise in the pressure reduces the replication quality back. Figure 8B shows that variation in vibration time and pressure impacts the replication quality of 300-μm-wide channels (AR = 1) as observed for 1000-μm-wide channels. When embossing channels of 100-μm-width (AR = 3) (Figure 8C), increasing vibration time and pressure monotonically reduces the replication quality. Regarding the interplay between vibration time and pressure, it appears that these parameters interact when replicating channels of any width and aspect ratio.

However, noting that *r* is confined in a very narrow range, we tested the statistical significance of the

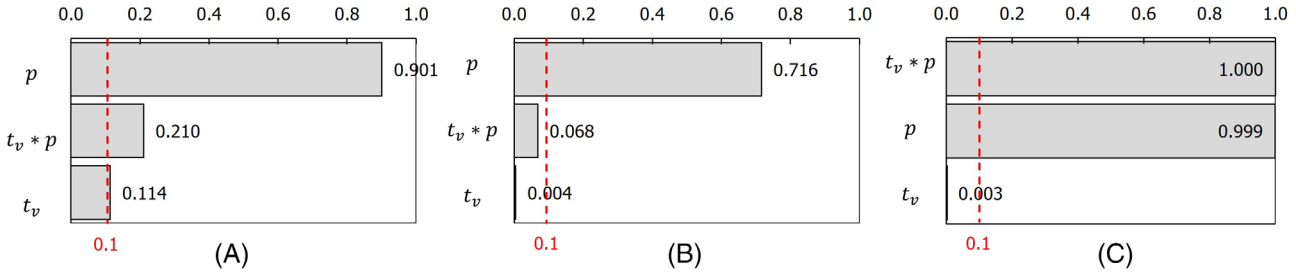

FIGURE 9 Pareto chart of the standardized effects on cross-correlation r for a confidence level of $\alpha = 0.1$ for (A) 1000-μm-wide (AR = 1/3), (B) 300-μm-wide (AR = 1), and (C) 100-μm-wide (AR = 3) wide channels. Dashed red line denotes the p-value corresponding to $\alpha = 0.1$ for $(a)(b)(n) - 1 = 26$ degrees of freedom, where $a = 3$ is the number of pressure levels, $b = 3$ is the number of vibration time levels, and $n = 3$ is the number of replications.

variation in cross-correlation. For this purpose, a two-way analysis of variance (ANOVA) was implemented across three replicated sets, aiming to investigate the statistical significance of the variations. Mean and the variance of the cross-correlations were computed for each combination of pressure and vibration time. Subsequently, a two-way ANOVA was conducted, yielding F-statistics that compare the variation in r within a group of samples (i.e., the replicates obtained with a specific parameter set) and the variation between the groups. The F-statistics were utilized to derive associated p-values, which were compared against a selected confidence level of $\alpha = 0.1$ to ascertain the significance of the effects. Figure 9 illustrates the Pareto chart showing the p-values computed for each parameter and their interaction. According to two-way ANOVA, the p-values smaller than $\alpha = 0.1$ indicate that the variation in cross-correlation is unlikely random and, thus, is significant. Consequently, it can be inferred that the effect of vibration time on the replication quality is statistically significant for all channel widths and aspect ratios, except 1000-μm-wide channels (AR = 1/3), where the effect of vibration time on replication quality appears to be marginally insignificant. Notably, interaction between pressure and vibration time has a statistically significant effect only for 300-μm-wide channels (AR = 1). Conversely, ANOVA indicates that the effect of pressure is statistically insignificant in replicating any channel.

To confirm the abovementioned observations, we referred to the more sensitive figure of merit, r_d. Variations in r_d caused by pressure, vibration time, and their interactions are presented in Figure 10. Comparing Figures 8 and 10 shows that the trends of the individual and combined effects of vibration time and pressure came out to be mostly the same with a difference in replicating 100-μm-wide channels, where an initial increase in vibration time slightly enhances the replication quality but further increase causes a reduction of r_d. The same trend is observed also for the pressure in replicating 100-μm-wide channels. To verify the significance of these effects, we again carried out an analysis of variance (Figure 11). Results support the conclusion that the effect of vibration time is statistically significant within $\alpha = 0.1$ for 100-μm-wide and 300-μm-wide channels. Similarly, consistent with the findings in Figure 9, interaction of vibration time and pressure is statistically significant in replicating 300-μm-wide channels. In addition, utilizing r_d pronounces the vibration time in replicating 1000-μm-wide channels, rendering its effect marginally significant. Conversely, in contrast to the results depicted in Figure 9, the significance of pressure effect and interactive effect of the parameters becomes noticeable for 100-μm-wide channels (AR = 3).

A closer analysis of Figures 9 and 11 reveals that the use of r_d not only differentiates lower and higher quality of replications but also clarifies the distinction between relative significance of the process parameters. Referring to Figure 11, it can be deduced that the individual and interaction effects of the parameters are pronounced more with decreasing channel width, hence increasing aspect ratio. On the other hand, in replicating any of the channels, individual effect of pressure is the least insignificant, while the interaction between pressure and vibration time is more effective on the replication quality. This interaction is more effective in replicating narrower channels with higher aspect ratios. Therefore, examining Figure 10B,C, it can be inferred that, when replicating relatively narrow and high aspect ratio channels with moderate vibration times, an initial rise in the pressure enhances the replication quality. However, excessive pressure is detrimental to the quality. Conversely, under low vibration times, increase in pressure consistently reduces the replication quality. In case of relatively high vibration times, pressure increase initially reduces the quality slightly, but a further increase improves it. This interplay between the vibration time and the pressure can be attributed to counteractions caused by the parameters. Vibration time has been experimentally proven to

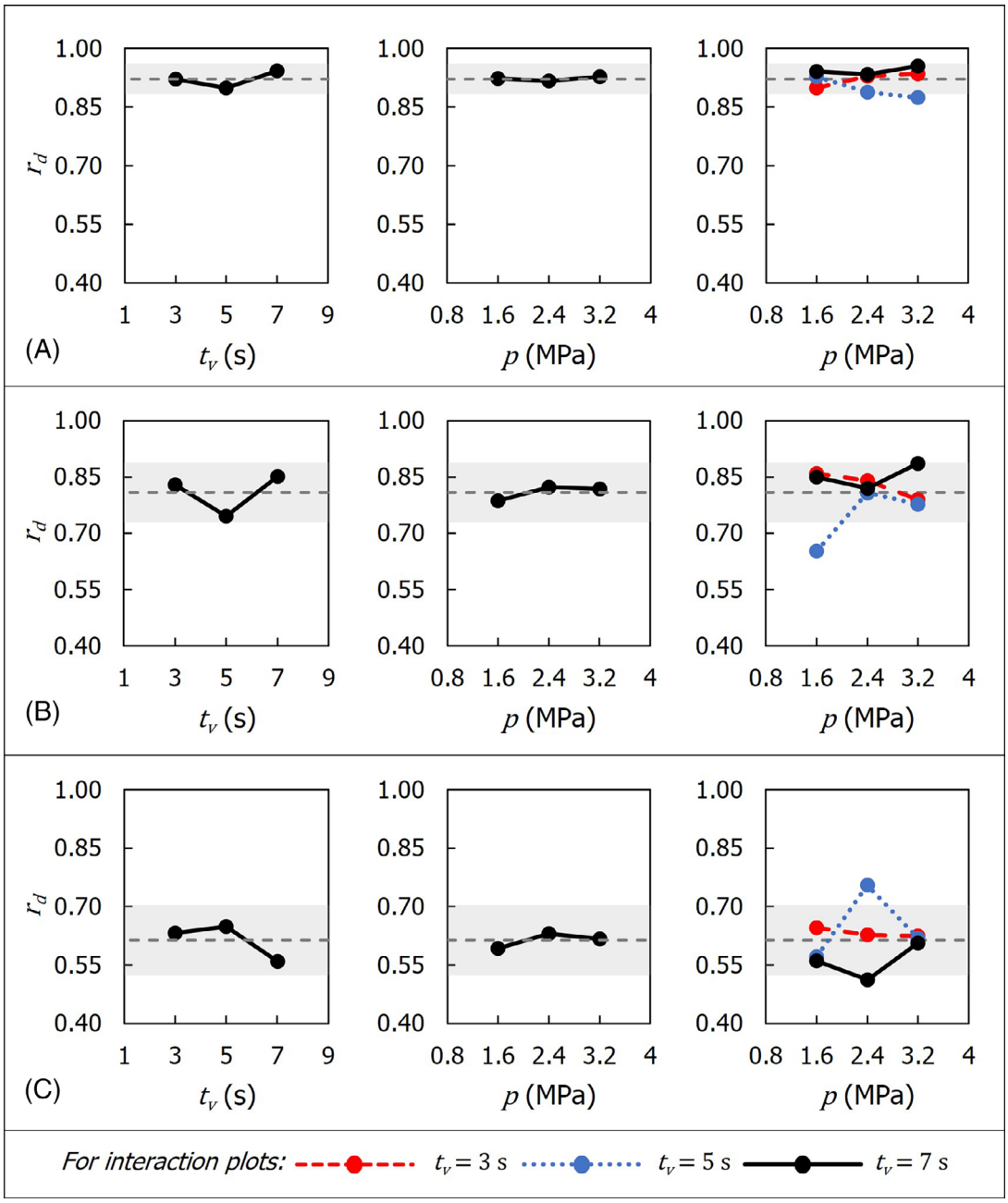

FIGURE 10 Main effects and interaction plots showing the relation between the cross-correlation r_d and the process parameters for (A–C) 1000-μm-wide channels (AR: 1/3), (d-f) 300-μm-wide channels (AR: 1), and (G–I) 100-μm-wide channels (AR: 3). Dashed lines indicate the average of the cross-correlation values for each channel width, while the gray band around the average indicates the standard deviations.

increase the temperature at the vicinity of the features on the mold, consequently enlarging the process-affected zone, within which the substrate material exceeds the glass transition and getting softer.[13] On the other hand, although the pressure mainly assists the softened material flow through and fills in the mold feature, it has been argued that it suppresses the friction effect by disturbing the progression of the vibrations to the substrate–mold interface.[9] Examining Figure 10B,C shows that apparently, at low vibration times, the suppressive effect of pressure over vibration is more pronounced in embossing moderate or narrow width channels with relatively higher aspect ratios; thus, the substrate cannot be heated enough, and the pressure becomes insufficient to make the material flow through the mold features. On the other hand, as the vibration time increases, the vibration starts dominating the process, causing an initial rise in the replication quality. However, excessive pressure seemingly restrains the vibration, thus reducing the quality. Further increasing the vibration time seemingly dominates over

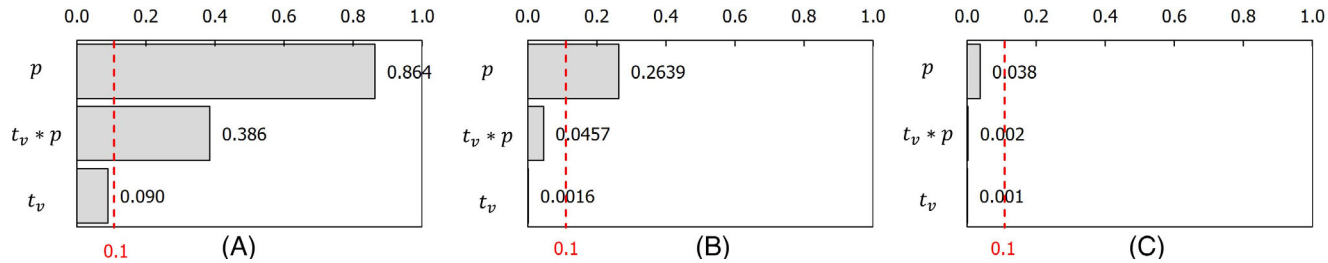

FIGURE 11 Pareto chart of the standardized effects for a confidence level of $\alpha = 0.1$ for (A) 1000-μm-wide (AR = 1/3), (B) 300-μm-wide (AR = 1), and (C) 100-μm (AR = 3)-wide channels. The response is the cross-correlation r_d. Dashed red line denotes the p-value corresponding to $\alpha = 0.1$ for $(a)(b)(n) - 1 = 26$ degrees of freedom, where $a = 3$ is the number of pressure levels, $b = 3$ is the number of vibration time levels, and $n = 3$ is the number of replications.

the effect of pressure restraining the vibration; thus, the replication quality could be improved even at higher pressures. On the other hand, in replicating wider channels with lower aspect ratios (Figure 10A), neither the pressure nor its interaction with the vibration time is effective on the result. In addition, the vibration time is only marginally effective in replicating the same channels with a tendency to improve the replication quality.

In addition to the statistical analysis on the relative effects of the individual and combined effects of the parameters, examination of Figure 10 reveals that the average of r_d across all cases is approximately 0.8. Referring to this average as a threshold, it can be suggested that r_d should be greater than 0.8 as a general rule for successful replication in ultrasonic embossing. Therefore, it can be concluded that 1000-μm-wide channels (AR = 1/3) could be replicated successfully, while 100-μm-wide channels (AR = 3) could not be replicated successfully, regardless of parameter combination. On the other hand, in replicating 300-μm-wide channels (AR = 1), the vibration time and the pressure should be selected with care to ensure a successful replication.

4 | CONCLUSION

To the best of our knowledge, for the first time in the literature, we propose a method to assess the replication quality in ultrasonic embossing of microchannels by considering the whole profile of the replicated feature instead of respecting a single dimension, such as the depth of the feature measured at a single location. The method emphasizes the fidelity of the fabricated features with the mold. Noting that the surface profile of the fabricated channels and the targeted channels resembles time series, with the difference that the series is not temporal but spatial, we utilized the cross-correlation function commonly used for signal processing purposes. As an improved method, we proposed calculating the cross-correlation by utilizing the derivatives of the target and fabricated profiles, which provides a more sensitive method for replicating the side walls, which are particularly crucial in microchannels as typically vertical side walls are required in microfluidic applications. Although we have used this approach to assess the ultrasonic embossing process, it can be utilized to assess any mold-based manufacturing method.

Regarding the replication quality of ultrasonic embossing, based on the experiment results, it can be stated the cross-correlation between the derivatives of the fabricated and target profiles should be greater than 0.8 for successful replication as a rule. Based on the experimental data, it can be concluded that ultrasonic embossing is not feasible for replicating relatively narrower channels with higher aspect ratios (AR > 1) as the cross-correlation between the derivatives of the profiles was always less than 0.8 regardless of the process parameters. However, for wider channels with low aspect ratios (AR < 1), ultrasonic embossing always resulted in cross-correlation values greater than 0.8, irrespective of the process parameters. In ultrasonic embossing of the channels with moderate width and a unit aspect ratio, the vibration time, and its combination with the pressure should be precisely selected to achieve an acceptable replication quality.

The experimental analysis provides reference data for replicating channels of varying width and aspect ratio. On the other hand, noting that ultrasonic embossing process relies on the heat generation through friction at the substrate–mold interface, future research could be directed toward investigation of the effect of surface roughness of the mold on replication quality.

A limitation is that two different means, namely scanning confocal microscopy for the mold and image processing of the cross-sections for the embossed features, have been utilized in measuring the profiles, which introduces a loss of accuracy due to mismatch of the measurement resolutions. As a measure, we have corrected this mismatch by resampling the profile data of both the mold and the channels with same spatial resolution. However,

utilizing a unified high-resolution method for both the mold and the channel would improve the accuracy in calculating the cross-correlation values.

Besides the statistical analysis presented in this work, referring to the results, it is evident that the fundamentals underlying the process still require attention and a comprehensive analytical or numerical model needs to be developed to describe the underlying physics. Our group is currently working on modeling of the process considering the interactions between the mold, substrate, horn, and the equipment.

ACKNOWLEDGMENTS

The authors would like to thank Assoc. Prof. Dr. M. Bülent Özer and Mr. M. Akif Şahin for laser Doppler vibrometry measurements, Prof. Dr. Barbaros Çetin and Mr. Can Güven for digital microscopy images, and Mr. Mehmet Oğulcan Güngör for ultrasonic embossing experiments and image processing.

FUNDING INFORMATION

This work was supported by the Scientific Research Projects Coordination Unit of Middle East Technical University (Grant no. GAP-302-2018-2757) and by the Scientific and Technological Research Council of Turkey (Grant no. 121M427).

DATA AVAILABILITY STATEMENT

The data that support the findings of this study are available from the corresponding author upon reasonable request.

ORCID

Ender Yildirim https://orcid.org/0000-0002-7969-2243

REFERENCES

1. Sia SK, Whitesides GM. Microfluidic devices fabricated in poly(dimethylsiloxane) for biological studies. *Electrophoresis*. 2003;24(21):3563-3576.
2. Guckenberger DJ, de Groot TE, Wan AM-DD, Beebe DJ, Young EWK. Micromilling: a method for ultra-rapid prototyping of plastic microfluidic devices. *Lab Chip*. 2015;15(11):2364-2378.
3. Gonzalez G, Roppolo I, Pirri CF, Chiappone A. Current and emerging trends in polymeric 3D printed microfluidic devices. *Addit Manuf*. 2022;55:102867.
4. Ma X, Li R, Jin Z, Fan Y, Zhou X, Zhang Y. Injection molding and characterization of PMMA-based microfluidic devices. *Microsyst Technol*. 2020;26(4):1317-1324.
5. Attia UM, Marson S, Alcock JR. Micro-injection moulding of polymer microfluidic devices. *Microfluid Nanofluidics*. 2009;7(1):1-28.
6. Peng L, Deng Y, Yi P, Lai X. Micro hot embossing of thermoplastic polymers: a review. *J Micromech Microeng*. 2014;24(1):13001.
7. Chen Q, Zhang L, Chen G. Far infrared-assisted embossing and bonding of poly(methyl methacrylate) microfluidic chips. *RSC Adv*. 2014;4(99):56440-56444.
8. Deshmukh SS, Goswami A. Experimental investigation of replication accuracy of polymer-based microfluidic chip fabricated through induction-assisted hot embossing and parametric optimization through nature-inspired algorithms. *Proceed Instit Mech Eng Part E J Proc Mech Eng*. 2023;0(0):1-17.
9. Mekaru H, Goto H, Takahashi M. Development of ultrasonic micro hot embossing technology. *Microelectron Eng*. 2007;84(5–8):1282-1287.
10. Schomburg WK, Burlage K, Gerhardy C. Ultrasonic hot embossing. *Micromachines*. 2011;2(4):157-166.
11. Sackmann J, Burlage K, Gerhardy C, Memering B, Liao S, Schomburg WK. Review on ultrasonic fabrication of polymer micro devices. *Ultrasonics*. 2015;56:189-200.
12. Liu SJ, Dung YT. Hot embossing precise structure onto plastic plates by ultrasonic vibration. *Polym Eng Sci*. 2005;45(7):915-925.
13. Sucularli F, Arikan MAS, Yildirim E. Investigation of process-affected zone in ultrasonic embossing of microchannels on thermoplastic substrates. *J Manuf Process*. 2020;50:394-402.
14. Kosloh J, Sackmann J, Šakalys R, Liao S, Gerhardy C, Schomburg WK. Heat generation and distribution in the ultrasonic hot embossing process. *Microsyst Technol*. 2017;23(5):1411-1421.
15. Tan JL, Lin WJ, Lam YC. Finite element simulation of ultrasonic embossing on polymers. *2014 13th Intern Conf Control Autom Robot Vision, ICARCV 2014*. 2014;2014(December):1229-1233.
16. Kosloh J, Sackmann J, Schomburg WK. Ultrasonic fabrication of micro fluidic channels from polyether ether ketone (PEEK). *Microsyst Technol*. 2017;23(12):5505-5513.
17. Liu SJ, Huang YC, Yang SY, Hsieh KH. Rapid fabrication of surface-relief plastic diffusers by ultrasonic embossing. *Opt Laser Technol*. 2010;42(5):794-798.
18. Hopmann C, Höfs C, Schomburg WK, Kosloh J, Sackmann J. Development of thermoplastic films for ultrasonic manufacturing of printed circuit boards. *Adv Polym Technol*. 2018;37(8):3460-3473.
19. Li J, Gerhardy C, Schomburg WK. Polymer circuit boards fabricated by ultrasonic hot embossing. *J Micromech Microeng*. 2013;23(7):075028.
20. Qi N, Luo Y, Yan X, Wang X, Wang L. Using silicon molds for ultrasonic embossing on polymethyl methacrylate (PMMA) substrates. *Microsyst Technol*. 2013;19(4):609-616.
21. Zhu J, Tian Y, Yang C, et al. Low-cost and fast fabrication of the ultrasonic embossing on polyethylene terephthalate (PET) films using laser processed molds. *Microsyst Technol*. 2017;23(12):5653-5668.
22. Fang-Yu F, Hsin-Chung C, Chiung-Fang H, et al. Replicability of process conditions of ultrasonic hot embossing for micropattern fabrication on thermoplastic substrates. *J Manuf Process*. 2020;60:283-291.
23. Qi N, Luo Y, Wang XD, Wang LD, Zhang ZB. Local thermal-assisted ultrasonic embossing for the fabrication of polymer microstructures. *Microsyst Technol*. 2015;21(5):1101-1110.
24. Luo Y, Yan X, Qi N, Wang X, Wang L. Study of double-side ultrasonic embossing for fabrication of microstructures on thermoplastic polymer substrates. *PLoS One*. 2013;8(4):e61647.

25. Li S, Xu Z, Reading I, Yoon SF, Fang ZP, Zhao J. Three dimensional sidewall measurements by laser fluorescent confocal microscopy. *Opt Express*. 2008;16(6):4001-4014.
26. Gülçür M, Romano JM, Penchev P, et al. A cost-effective process chain for thermoplastic microneedle manufacture combining laser micro-machining and micro-injection moulding. *CIRP J Manuf Sci Technol*. 2021;32:311-321.
27. Vera J, Brulez AC, Contraires E, et al. Factors influencing microinjection molding replication quality. *J Micromech Microeng*. 2018;28(1):15004.
28. Piccolo L, Puleo K, Sorgato M, Lucchetta G, Masato D. Modeling the replication of submicron-structured surfaces by micro injection molding. *Mater Des*. 2021;198:109272.
29. Zerehsaz Y, Shao C, Jin J. Tool wear monitoring in ultrasonic welding using high-order decomposition. *J Intell Manuf*. 2019; 30(2):657-669.
30. Fong KM, Wang X, Kamaruddin S, Ismadi MZ. investigation on universal tool wear measurement technique using image-based cross-correlation analysis. *Measurement*. 2021;169: 108489.
31. Sukeri M, Paiz Ismadi MZ, Othman AR, Kamaruddin S. Wear detection of drill bit by image-based technique. *IOP Conf Ser Mater Sci Eng*. 2018;328(1):12011.
32. Perris J, Kumar C, Xu Y, et al. 3D printing and rapid replication of advanced numerically generated rough surface topographies in numerous polymers. *Adv Eng Mater*. 2023; 25(1):1-14.
33. Kumar C, Palacios A, Surapaneni VA, et al. Replicating the complexity of natural surfaces: technique validation and applications for biomimetics, ecology and evolution. *Philosophic Trans Roy Soc A Mathematic Phys Eng Sci*. 2019; 377:20180265.
34. Arcot Y, Samuel GL, Kong L. Micro hot-embossing of serpentine channels on PMMA based microfluidic devices. Proceedings of 10th International Conference on Precision, Meso, Micro and Nanoengineering (COPEN 10), 1044–1047. 2017.
35. Çoğun F, Yıldırım E, Arikan MAS. Investigation on replication of microfluidic channels by hot embossing. *Mater Manuf Process*. 2017;32(16):1838-1844.

How to cite this article: Yildirim E, Ulku MK, Arikan MAS. Utilization of cross-correlation function for assessment of replication quality in ultrasonic embossing of microchannels on polymethyl methacrylate. *Polym Eng Sci*. 2024;1-16. doi:10.1002/pen.26764